

DECLARATION

I declare that this thesis is my own, unaided work. It is being submitted for the degree of Doctor of Philosophy in the University of the Witwatersrand, Johannesburg. It has not been submitted before for any degree or examination in any other University.

.....

(Signature of candidate)

..... day of2005

ABSTRACT

The main aim of this thesis has been to study the way in which Fe(III) and Co(II) incorporation into Si-MCM-41 synthesis gels affects the properties of the unmodified material. Another aim was to investigate the influence of these hetero-atoms on the dispersion and particle size distribution as well as the catalytic activity of supported Au nanoparticles in the CO oxidation reaction.

Si-MCM-41 has been successfully synthesized in this work using mixtures containing CTAB as a structure-directing agent (SDA) and water-glass as a SiO₂ source. Replacement of water-glass with pre-calcined Si-MCM-41 for SiO₂ source in the secondary synthesis step has produced Si-MCM-41 with improved structural properties (XRD, HRTEM and Raman spectroscopy), including restructured and more crystalline pore walls (Raman spectroscopy).

The conventional shortcomings of Si-MCM-41 as a support for catalytically-active (transition) metal components such as low hydrothermal stability, low PZC, lack of cation exchange capacity and no reducibility have been partially addressed by modification with Fe(III) and Co(II). The premodification was achieved both during framework synthesis and after synthesis by the incipient wetness impregnation (IWI) method. As opposed to the one-pot synthesis of metal-containing derivatives, the IWI method gave materials with high metal loadings and maximal retention of the properties of pristine Si-MCM-41. On the other hand, metal incorporation during synthesis to a loading of ~8.8 wt% using aqueous solutions of metal precursors showed some collapse of the mesostructure. Consequently methods were sought to incorporate this amount of metal (and up to double, i.e., 16 wt%) with maximal retention of the MCM-41 characteristics. These methods included (i) using Si-MCM-41 as a SiO₂ source, (ii) dissolving the metal precursors in an acid solution before inclusion into the synthesis gel, and (iii) using freshly precipitated alkali slurries of the metal precursors. The first method produced a highly ordered 16wt% Fe-MCM-41 material with excellent reducibility (TPR showed three well-resolved peaks) and pore-wall structure (Raman spe-

ctroscopy). Like the aqueous route, the acid-mediated metal incorporation route did not produce ordered materials at metal contents of ~16 wt%. The base precipitate route produced highly ordered composite materials up to 16 wt% metal content, with characteristics similar to those of Si-MCM-41 (XRD, BET and HRTEM), although some metal phases were observed as a separate phase on the SiO₂ surface. Thus, metal-containing MCM-41 materials could be obtained with conservation of MCM-41 mesoporosity. Raman spectroscopic studies have shown that the effect of transition metal incorporation in MCM-41-type materials is to strengthen the pore walls (shift of Si-O-Si peaks to higher frequencies), while TPR studies revealed that the essentially neutral framework of Si-MCM-41 could be rendered reducible by transition metal incorporation.

Gold-containing mesoporous nanocomposites were prepared by both direct synthesis and post-synthetically. Catalysts prepared by direct hydrothermal synthesis were always accompanied by formation of large Au particles because of the need to calcine the materials at 500 °C in order to remove the occluded surfactant template. The presence of transition metal components in Me-MCM-41 (Me = Fe and Co) has been found to play a significant role in the particle size distribution and also the dispersion of Au nanoparticles when these materials were used as supports. In general, a base metal-containing support was found to produce smaller Au nanoparticles than the corresponding siliceous support. It has been proposed that the transition metal components serve as anchoring or nucleation sites for the Au nanoparticles, which are likely to sinter during calcination. The anchoring sites thus retard the surface mobility of Au at calcination temperatures above their T_{Tammann} .

The use of the Au/Me-MCM-41 materials as catalysts in the CO oxidation reaction has led to the following observations: (i) catalyst on metal-containing supports showed better activity than those on Si-MCM-41, probably due to the induced reducibility in metal-MCM-41, (ii) catalysts prepared by direct synthesis showed inferior activity owing to large Au particles, (iii) increasing Au content improves the catalytic performance, (iv) increasing the Fe content of the support

at constant Au improves the catalytic performance, and (v) changing the base metal component of the support from Fe to Co led to a significant improvement in catalytic activity. The similarity of the apparent activation energies (E_a) for the 5 wt% Au-containing 5 wt% Fe- and 5 wt% Co-MCM-41 suggested that the difference in catalytic activity is associated with the number of active sites possessed by each catalyst system. The observed order of catalytic activity of these 5 wt% Au-containing systems in terms of the support type is: Co-MCM-41 > Fe-MCM-41 > Si-MCM-41. This was further supported by the average Au particle size, which, in terms of the support, followed the order Co-MCM-41 < Fe-MCM-41 < Si-MCM-41. Thus, metal-support interactions between Au and MCM-41 have been enhanced by introducing Fe(III) and Co(II), which also induced framework charge, ion exchange capacity (IEC) and reducibility in the neutral siliceous support.

DEDICATION

This thesis is dedicated to the memory of my brother

Malesela Simon Mokhonoana

1970-2003

ACKNOWLEDGEMENTS

The extract from the late Brenda Fassie's song, "*It's nice to be with people*" is key to success in life, because whatever we achieve in life depends on how we interact with each other. I would not have accomplished this work without the help from other people, and my sincere appreciation goes to the following people and institutions:

My supervisor, Prof. N. J. Coville for his patience, guidance, support and suggestions

Mr. Basil Chassoulas for his assistance with the autoclaves and TPR measurements

Messrs. Barry Fairbrother and Steve Ganon for their remarkable glassblowing, fixing and making my TPR reactors.

Manuel Fernandes and Prof. Schoning for their continued assistance with the XRD diffractometer, all the pains of changing receiving slits to adapt for low-angle scans.

Prof. Abhaya K. Datye of the Chemical Engineering Department, University of New Mexico, Albuquerque, USA, for giving me the opportunity to research in his Group. Assistance from Hien Pham (*Post-doc*) and Mangesh Bore (*PhD student*) is also appreciated. Your guidance and suggestions are unforgettable.

Prof. Harold H. Kung of the Chemical Engineering Department, Northwestern University, Evanston (*Chicago*), USA, for giving me a further research opportunity in his Group. Being with you was a pleasant research experience, and your approach to research will always be remembered.

My parents, brothers and sisters for their support, encouragement and assistance (*particularly Dr. Moses during my stay in the USA*).

The NRF (*through the Staff Development Program*) and the University of the Witwatersrand for financial support

The NRF-NSF joint support for financing my visit and studies in the United States of America

Last but not least, I would like to thank the University of the North for allowing me study leave for the period 2000-2002.

TABLE OF CONTENTS

	<u>Page</u>
DECLARATION	i
ABSTRACT	ii
DEDICATION	v
ACKNOWLEDGEMENTS	vi
TABLE OF CONTENTS	viii
LIST OF FIGURES	xvi
LIST OF TABLES	xxix
LIST OF ABBREVIATIONS AND ACRONYMS	xxxii
SCOPE AND CONTENT OF THE THESIS	xxxvii
APPENDICES	357
CHAPTER 1: GENERAL INTRODUCTION	
1.1 Extension from Microporous to Mesoporous Dimensions	1
1.2 Synthesis and Fabrication of Mesoporous MCM-41	5
1.2.1 Liquid-Crystal Templating: Supramolecular Self-Assembly	5
1.2.2 Sol-Gel Synthesis Route (Alkali-free Synthesis)	7
1.2.3 Other Mesoporous Materials: Post-LCT Syntheses	9
1.2.3.1 Silica-Based Mesoporous Materials	9
1.2.3.2 Metal Oxide-Based Mesoporous Materials	14
1.2.3.3 Carbon-Based Mesoporous Materials	15
1.2.4 Methods of Template Removal from the Mesostructure	17
1.3 Characteristics of Mesoporous Materials (MCM-41)	18
1.3.1 Bulk and Textural features of MCM-41	18

1.3.2 Morphologies and Shapes in Mesoporous MCM-41 Materials	21
1.3.3 Hydrothermal stability of MCM-41 Materials	22
1.3.3.1 Improving the thermal/hydrothermal stability of Si-MCM-41	23
1.4 Catalysis and Technical Applications of MCM-41 Materials	26
1.4.1 Organically-Modified MCM-41 Materials	26
1.4.1.1 Co-condensation or Direct Organic Modification of MCM-41	28
1.4.1.2 Post-synthesis Organic Modification of MCM-41	28
1.4.1.3 Decontamination of Ground Water: Heavy Metals and Oxyanions	29
1.4.2 Metal-containing Mesoporous Materials (Me-MCM-41)	34
1.4.2.1 Iron-containing Mesoporous MCM-41 (Fe-MCM-41)	35
1.4.2.2 Cobalt-containing Mesoporous MCM-41 (Co-MCM-41)	39
1.4.3 General Catalytic Reactions of Mesoporous Materials	45
1.5 Pollution Control Through Catalysis	46
1.5.1 Carbon Monoxide Poisoning	47
1.5.2 CO Oxidation and Catalysis by Gold	48
1.5.3 Commercial Applications of Gold Catalysts	51
1.5.4 Supported Au Catalysts	51
1.5.5 Preparation of Supported Au Catalysts	54
1.5.6 Controversy over the Active species in CO Oxidation	58
1.6 Hypotheses and Aims of the Study	59
1.7 Rationale/Motivation for Research in this Thesis	60
1.8 References	63
CHAPTER 2: MESOPOROUS SILICA MCM-41 (Si-MCM-41)	
2.1 Introduction	95

2.1.1 Synthesis of MCM-41	96
2.2 Experimental section	99
2.2.1 Starting materials (chemicals, stock solutions and solvents)	99
2.2.2 Synthesis of the Si-MCM-41 Material (Procedure)	99
2.2.2.1 Unstirred Synthesis of Si-MCM-41	100
<i><u>Room Temperature Synthesis of Si-MCM-41</u></i>	100
<i><u>Hydrothermal Synthesis of Si-MCM-41</u></i>	100
2.2.2.2 Stirred Synthesis of Si-MCM-41	102
2.2.3 Characterization of Si-MCM-41	102
2.2.3.1 X-ray Powder Diffraction	102
2.2.3.2 BET surface area measurement	103
2.2.3.3 HRTEM studies of Si-MCM-41	103
2.3 Results and Discussion	103
2.3.1 Structural (Bulk) Characterization of Si-MCM-41 (XRD)	104
2.3.1.1 Room Temperature Synthesis	104
2.3.1.2 Hydrothermal Synthesis	113
2.3.1.3 Al-Si-MCM-41 Studies	131
2.3.2 BET surface area measurements	134
2.3.2.1 Room Temperature Synthesized Si-MCM-41 Materials	134
2.3.2.2 Hydrothermally-prepared Si-MCM-41 Materials	136
2.3.3 High Resolution Transmission Electron Microscopy (HRTEM) Studies	141
2.4 Conclusions	147
2.5 References	152

CHAPTER 3: IRON- AND COBALT-CONTAINING MCM-41: Synthesis and Characterization

3.1 Introduction	155
3.1.1 Probing the Fe environment in Fe-MCM-41 using ESR spectroscopy	158
3.1.2 Temperature-Programmed Reduction (TPR)	161
3.1.3 Synthetic Strategies used in this study	162
3.2 Experimental	162
3.2.1 Starting Materials	162
3.2.2 Synthesis Procedure	163
(a) <i>Direct Synthesis: (Aqueous) Acid-mediated route</i>	164
(b) <i>Direct Synthesis: The hydroxide precipitate route</i>	164
(c) <i>Post-synthesis metal incorporation: Incipient Wetness Impregnation</i>	164
3.2.3 Characterization of Fe- and Co-MCM-41	165
(a) <i>X-ray Powder Diffraction (XRD)</i>	165
(b) <i>BET Surface Area Measurements</i>	165
(c) <i>High Resolution Transmission Electron Microscopy (HRTEM)</i>	165
(d) <i>Energy-Dispersive Spectrometry (EDS)</i>	166
(e) <i>Temperature-Programmed Reduction Using Hydrogen (H₂-TPR)</i>	166
(f) <i>Electron Spin Resonance (ESR) Spectroscopy</i>	166
(g) <i>Raman Spectroscopy</i>	167
(h) <i>Infrared Spectroscopy</i>	167
3.3 Results and Discussion	167
3.3.1 X-ray Powder Diffraction (XRD and BET) measurements	167
(a) <i>Incipient wetness impregnation (IWI) with Fe or Co Precursors</i>	168
(b) <i>Direct Incorporation of aqueous Fe(III) and Co(II) During Synthesis</i>	173

<i>(c) Acid Mediated Incorporation of Fe during synthesis</i>	178
<i>(d) Acid-Mediated Incorporation of Co</i>	183
<i>(e) Simultaneous Incorporation of Fe and Co by the Acid-Mediated Route</i>	184
<i>(f) Base-Mediated Incorporation of Fe During Synthesis</i>	185
1. <i>Variation of the type of base used</i>	185
2. <i>Iron content</i>	187
3. <i>Temperature</i>	188
<i>(g) Base-mediated incorporation of Co</i>	190
<i>(h) Comparisons between Me-MCM-41 (Me = Fe, Co, Ru) prepared by the base precipitate</i>	194
3.3.2 High Resolution Transmission Electron Microscopy (HRTEM)	196
3.3.3 Temperature-Programmed Reduction (TPR)	202
3.3.3.1 TPR studies of Fe-containing MCM-41	202
3.3.3.2 TPR studies of Co-containing MCM-41	212
3.3.3.3 TPR studies of bimetallic-derivatized MCM-41	215
3.3.4 Spectroscopic Methods	217
3.3.4.1 Electron Spin Resonance (ESR or EPR) Spectroscopy	217
3.3.4.2 Raman Spectroscopy	225
3.3.4.3 Infrared Spectroscopy	233
3.4 Conclusions	235
3.5 References	240
CHAPTER 4 SYNTHESIS AND CHARACTERIZATION OF Au-CONTAINING Me-MCM-41 (Me = Si, Co, Fe)	
4.1 Introduction	247
4.1.1 Synthesis of Supported Gold Nanoparticles: General	249

4.1.2 Gold Nanoparticles on Haruta-type Supports	249
<i>(i) Coprecipitation (CP)</i>	251
<i>(ii) Deposition-precipitation (DP)</i>	252
4.1.3 Gold Nanoparticles on Conventional Zeolite Supports	252
4.1.4 Gold Nanoparticles on Mesoporous Zeolite Supports	253
4.1.5 Characterization of Supported Gold Nanoparticles	254
4.1.6 Aim of Study	256
4.2 Experimental	257
4.2.1 Materials	257
4.2.2 Synthesis of Mesostructured Au/Me-MCM-41 (Me = Si, Co, Fe)	257
4.2.2.1 One-pot Synthesis of Au-containing MCM-41: Direct 80-100 °C Synthesis	258
4.2.2.2 Post-synthesis Approach to Au-containing MCM-41: Ethylenediamine route	258
4.2.2.3 Post-synthesis Approach to Au-containing MCM-41: Coprecipitation route	259
4.2.2.4 Post-synthesis Approach to Au-containing MCM-41: Miscellaneous	259
4.2.3 Characterization of Au/Me-MCM-41 (Me = Si, Fe, Co)	259
4.3 Results and Discussion	260
4.3.1 X-ray Diffraction Studies	260
4.3.2 BET Surface Area Measurements	264
4.3.3 High Resolution Transmission Electron Microscopy (HRTEM) Studies	267
4.3.3.1 Gold Incorporation by Direct Hydrothermal Synthesis (One-pot Synthesis)	267
4.3.3.2 Post-synthesis incorporation of Au in Mesoporous Supports	270

4.3.3.3 Gold Incorporation by Precipitation with ethylenediamine solution and calcinations	270
4.3.3.4 Gold Incorporation by other Methods (Post-synthetically)	280
4.4 Conclusions	287
4.5 References	291
CHAPTER 5: CO OXIDATION OVER Au/Me-MCM-41 (Me = Si, Fe, Co) MATERIALS	
5.1 Introduction	298
5.1.1 Gold Catalysts Supported on Mesoporous Silica Derivatives	302
5.2 Experimental	304
5.2.1 Starting Materials	304
5.2.2 Catalyst Preparations	305
Method A	305
Method B	305
Method C	306
5.2.3 Activity Testing Procedure	306
5.3 Results and Discussion	308
5.3.1 Gold Catalysts on Pure Silica MCM-41 Supports	308
5.3.2 Gold Catalysts on Co-functionalized Mesoporous Supports	312
5.3.3 Gold Catalysts on Fe-functionalized Mesoporous Supports	315
5.3.4 Gold catalysts on Fe-functionalized MCM-41: Ethylenediamine Synthesis route	317
5.3.5 Gold catalysts on Fe-functionalized MCM-41: Other Post-synthesis Methods	327
5.4 Conclusions	334
5.5 References	339

CHAPTER 6 SUMMARY AND CONCLUSIONS

6.1 Summary	343
6.2 Conclusions	345

APPENDICES

Appendix A.1. The XRD patterns of Si-MCM-41 materials prepared at 80 °C for 6 h under magnetic stirring. The ratio R_{SiO_2} represents $\text{mols}_{\text{SiO}_2}(\text{TEOS})$ divided by $\text{mols}_{\text{SiO}_2}(\text{water-glass})$ in the synthesis gel.	357
Appendix A.2. Table of lattice parameters of Si-MCM-41 (prepared at 100 °C for 2 days) as a function of the synthesis gel H_2O content	358
Appendix A.3. XRD pattern of 20 wt% Fe-MCM-41 prepared at 100 °C for 2 days via the OH^- precipitate route	359
Appendix A.4. XRD patterns of 16 wt% Fe-MCM-41 (100 °C, 2 d) using different precipitants (TEA and Na_2CO_3).	360
Appendix A.5 (i). The EDS spectrum of 5 wt% Au/14 wt% Fe-MCM-41 prepared via the (en) route on the Fe-rich support, followed by calcination at 380 °C for 6 h. Average particle size 3.55 nm.	361
Appendix A.5 (ii). EDS spectrum of 2.28 wt% Au/CTAB-MCM-41 prepared via the en route, and then calcined at 500 °C for 12 h to decompose the surfactant. Note that the Au content is relative to the as-synthesized material, and the actual Au content is actually higher than the stipulated value	361
Appendix A.6 Raw data for the CO oxidation reaction using 1.48 wt% Au.Co-MCM-41 as a catalyst, calcined at 325 °C for 6 h	362
Appendix A.7. The framework Raman spectrum of <i>sec</i> -Si-MCM-41 prepared at 100 °C for 48 h and then calcined at 560 °C for 6 h	363
Appendix A.8. Conferences Attended and Presentations	364

LIST OF FIGURES

CHAPTER 1

- Figure 1.1** Three structure types observed for silica-surfactant mesophases: (a) MCM-41 (Hexagonal, 1-D), (b) MCM-48 (Cubic, bicontinuous, 3-D), (c) MCM-50 (Lamellar, 2-D) **4**
- Figure 1.2** Liquid-crystal templating (LCT) mechanism for self-assembly proposed by Beck et al [26] showing two possible pathways for the formation of MCM-41: (1) liquid-crystal initiated and (2) silicate-initiated **6**
- Figure 1.3** SEM micrograph of SBA-2 showing different morphologies **12**
- Figure 1.4** (Left) Changes in powder XRD patterns during synthesis of the carbon molecular sieve CMK-1 with its silica template MCM-48: (a) The mesoporous silica molecular sieve MCM-48, (b) MCM-48 after completing carbonization within pores, and (c) CMK-1. (Right): Powder XRD patterns of CMK-3 carbon and SBA-15 silica used as template for the CMK-3 synthesis **16**
- Figure 1.5** TEM images of MCM-41 materials with Ar pore sizes of (a) 20, (b) 40, (c) 65 and (d) 100 Å **19**
- Figure 1.6** XRD pattern (a) of high-quality calcined MCM-41 reported by Huo et al [34], and N₂ adsorption isotherm (b) reported by Branton et al [127] **20**
- Figure 1.7** SEM images of (a) BMS-1, (b) BMS-2, and (c) BMS-3. The length of the bar for (a, b) corresponds to 5 μm and for (c) corresponds to 10 μm. Varying amounts of ethyl acetate were added to the synthesis mixture for the preparation of the BMS materials, with BMS-1, BMS-2 and BMS-3 prepared by adding 15, 25 and 35 ml, respectively, of ethyl acetate to the synthesis gel [ref. 144] **21**
- Figure 1.8** Powder XRD patterns of Si-MCM-41 and Si-Al-MCM-41 (a) before and (b) after treatment in boiling water for 1 week **25**
- Figure 1.9** S_{BET} of Si-MCM-41, Si-Al-MCM-41, and Al/Si-MCM-41 before and after treatment in boiling water for 1 week: ■ fresh sample, □ in boiling water. The last material was prepared by Al impregnation of Si-MCM-41 **25**
- Figure 1.10** Recipe for the formation of a silica sponge (A), and retention of the hexagonal structure (B) **31**
- Figure 1.11** Heavy metal removal by SAMMS **32**
- Figure 1.12** XRD patterns of Co/MCM-41 and MCM-41 **40**
- Figure 1.13** Zeta potential of MCM-41 as a function of pH. The dotted line indicates the isoelectric point **42**

- Figure 1.14** TPR patterns of CoMo/Al-MCM(*x*) catalysts, *x* is the weight % of MCM-41 in the support **43**
- Figure 1.15** TEM micrograph of Au-Fe (1 : 19) coprecipitate calcined at 400 °C: dispersion of gold over α -Fe₂O₃ **52**
- Figure 1.16** Conversions of H₂ and CO in catalytic oxidation reactions as a function of catalyst temperature. CO or H₂ 1 vol% in air, SV = 2 × 10⁴ h⁻¹.ml/g-cat: oxidation of H₂ (○) and CO (●) on Au-Fe (1 : 19) coprecipitate calcined at 400 °C in air; oxidation of H₂ (□) and CO (■) on Au powder prepared from colloidal metal particles with diameters around 20 nm; oxidation of H₂ (Δ) and CO (▲) on α -Fe₂O₃ powder prepared by calcination of ferric hydroxide at 400 °C **53**
- Figure 1.17** Arrhenius plots for the rate of CO oxidation over supported catalysts: (▲) Au (1.2 wt%)/Co₃O₄, (□) Au (0.66 wt%)/ α -Fe₂O₃ and (○) Au (3.3 wt%)/TiO₂ **53**
- ## CHAPTER 2
- Figure 2.1** XRD patterns of Si-MCM-41 samples: Different batches prepared on different days using gels of the same composition (mean $a_0 = 46.7 \text{ \AA}$) **101**
- Figure 2.2** XRD patterns of Si-MCM-41 materials synthesized at room temperature for 47 days. Replicate syntheses were done using distilled water and deionized water as solvent media **105**
- Figure 2.3** XRD patterns of some Si-MCM-41 materials prepared at room temperature **106**
- Figure 2.4** XRD patterns of Si-MCM-41 made at RT using templates of different alkyl chain lengths: ^aC₁₄ represents tetradecyltrimethylammonium bromide, and C₁₆ represents cetyltrimethylammonium bromide (a.k.a. CTAB) **108**
- Figure 2.5** The XRD patterns of Si-MCM-41 prepared at RT from gels of varying silicon/surfactant ratios **110**
- Figure 2.6** Variation of the lattice parameter with synthesis gel H₂O content (RT, 5 days) **111**
- Figure 2.7** XRD patterns of secondary Si-MCM-41: (a) primary Si-MCM-41 (parent), and (b) 2^o synthesis at RT for 2 days **112**
- Figure 2.8** XRD pattern of Si-MCM-41 prepared by aging at RT for 5 days, with water-glass first titrated with HNO₃ prior adding to CTAB solution. Calcined at 560 °C for 6 h **113**

Figure 2.9 XRD patterns of Si-MCM-41 showing the effect of synthesis temperature (3 days synthesis)	114
Figure 2.10 A plot of a_0 versus synthesis temperature for Si-MCM-41, 3 days synthesis. Room temperature has been arbitrarily taken as 25 °C.	115
Figure 2.11 XRD patterns of Si-MCM-41 made from gels with different pH values (2 days)	116
Figure 2.12 The XRD pattern of Si-MCM-41 prepared by intermediate pH adjustment	117
Figure 2.13 XRD patterns of calcined Si-MCM-41 prepared at 100 °C for 12-72 h: (a) $1^\circ \leq 2\theta \leq 10^\circ$, and (b) $3^\circ \leq 2\theta \leq 10^\circ$ (higher order region)	118
Figure 2.14 Variation of a_0 with synthesis time at 100 °C for Si-MCM-41	119
Figure 2.15 XRD patterns of Si-MCM-41, RT v/s 100 °C synthesis: (a) 3 days, (b) 5 days	120
Figure 2.16 A plot of lattice parameter versus gel H ₂ O/SiO ₂ molar ratio (Si-MCM-41, 100 °C, 2 days)	121
Figure 2.17 XRD patterns of Si-MCM-41 prepared in a pH 10 buffer solution	121
Figure 2.18 XRD pattern of Si-MCM-41 prepared by doubling the gel composition	123
Figure 2.19 XRD patterns of Si-MCM-41 prepared using different acids	124
Figure 2.20 XRD patterns of Si-MCM-41 synthesized at 100 °C for 2 days	125
Figure 2.21 XRD patterns of Si-MCM-41, showing the effect of the silica precursor	126
Figure 2.22 XRD patterns of secondary Si-MCM-41: Effect of calcination temperature	127
Figure 2.23 The XRD patterns of secondary Si-MCM-41: Effect of synthesis time, (a) full range, and (b) $3^\circ \leq 2\theta \leq 10^\circ$	129
Figure 2.24 XRD pattern of Si-MCM-41 prepared by heating the synthesis gel (97 °C for 45 minutes) made with pre-hydrolysis of water-glass with HNO ₃ before adding to CTAB solution. Calcined at 560 °C for 6 h	130

Figure 2.25 XRD patterns of (Al, Si)-MCM-41 (Si/Al = 30) prepared at 100 °C for 48 h: (a) Al source added to the gel after pH adjustment, (b) Al source added to the gel before pH adjustment, followed by 2 days aging prior to synthesis, and (c) Al source added to the gel before pH adjustment **132**

Figure 2.26 XRD patterns of (Al, Si)-MCM-41 (Si/Al = 22) prepared by IWI of Si-MCM-41. (a) methanol as solvent, (b) water as solvent, and (c) ethanol as solvent. IWI abbreviates incipient wetness impregnation **133**

Figure 2.27 XRD patterns of (Al, Si)-MCM-41 (Si/Al = 22) by different synthesis routes **134**

Figure 2.28 Variation of the BET surface area of Si-MCM-41 with gel water content (RT, 5 days) **135**

Figure 2.29 Variation of the BET surface area with synthesis time for Si-MCM-41 (100 °C) **137**

Figure 2.30 HRTEM images of Si-MCM-41 prepared at 100 °C for 5 days, and calcined at 560 °C for 6 h **142**

Figure 2.31 HRTEM images of Si-MCM-41 made with CTAB/NaK-tartrate as template, calcined at 560 °C for 6 h: Images taken at different regions of the same sample **143**

Figure 2.32 Different regions of Si-MCM-41 (2 days, 100 °C, C₁₄TMAB as template, calcined at 560 °C for 6 h) as seen under HRTEM **144**

Figure 2.33 HRTEM images of different regions of Si-MCM-41 prepared at 80 °C for 6 h, R_{SiO₂} = 3.95, and calcined at 500 °C for 12 h **145**

Figure 2.34 HRTEM images of different regions of Si-MCM-41 prepared at 80 °C for 6 h, with R_{SiO₂} = 1.48, and calcined at 500 °C for 12 h **146**

CHAPTER 3

Figure 3.1 TEM micrograph of 4 wt% Fe-MCM-41. Fe introduced during framework synthesis **157**

Figure 3.2 Room temperature X-band EPR spectrum of the iron-containing Kenyaite **160**

Figure 3.3 XRD patterns of 5 wt% Fe-MCM-41 (a) and the pure support (b) **168**

Figure 3.4 The XRD pattern of 5 wt% Fe-MCM-41 prepared by IWI of *sec*-Si-MCM-41, calcined at 560 °C for 6 h. Insert: Expanded high-angle region, * represents Fe₂O₃ **169**

- Figure 3.5** XRD patterns of Fe-MCM-41 prepared by IWI compared with that of bulk Fe₂O₃: (a) 16 wt% Fe-MCM-41, (b) 50 wt% Fe-MCM-41, and (c) bulk Fe₂O₃ **171**
- Figure 3.6** XRD patterns of 16 wt% Co-MCM-41 prepared by IWI in 1 M HNO₃ solution (a) and Co₃O₄ reference sample (b) **172**
- Figure 3.7** Effect of Co incorporation by IWI on XRD patterns: (a) parent Si-MCM-41 and (b) 10.2 wt% Co-MCM-41 **172**
- Figure 3.8** Effect of synthesis gel pH on the XRD properties of hydrothermally-prepared 1.9 wt% Fe-MCM-41 **173**
- Figure 3.9** XRD patterns of 8.8 wt% Fe-MCM-41: Solid NaOH versus aqueous NaOH for pH adjustment **174**
- Figure 3.10** XRD pattern of 8.9 wt% Co-MCM-41 prepared at 100 °C for 72 h (one-pot synthesis) **175**
- Figure 3.11** Low-angle (a) and high-angle (b) XRD patterns of 16 wt% Fe-MCM-41: Fe³⁺(aq) added after 2 h stirring. Synthesis at 100 °C for 6 h, dried at 110 °C for 3 h, uncalcined **176**
- Figure 3.12** Variation of *a*₀ with calcination temperature for 5 wt% Fe-MCM-41 prepared at 100 °C for 2 days **178**
- Figure 3.13** XRD patterns of 5 wt% Fe-MCM-41 calcined at different temperatures **179**
- Figure 3.14** Lattice parameters for 8.8 wt% Fe-MCM-41 prepared at 100 °C for 2 days using various acids to add the Fe precursor **180**
- Figure 3.15** Variation of BET surface areas of 8.8 wt% Fe-MCM-41, prepared at 100 °C for 2 days, with acid identity. All samples were calcined at 560 °C for 6 h **181**
- Figure 3.16** Variation of the BET surface area (a) and lattice parameter (b) with Fe content for the Fe-MCM-41 materials prepared in HNO₃ at 100 °C for 48 h. All samples were calcined at 560 °C for 6 h **182**
- Figure 3.17** XRD patterns of a bimetallic and monometallic Fe-MCM-41 prepared at 100 °C for 2 days with metal precursors in 1 M HNO₃: (a) 8.8 wt% Fe-MCM-41 and (b) (7.8 wt% Fe, 11.5 wt% Co)-MCM-41 **184**
- Figure 3.18** XRD patterns of Fe-MCM-41 prepared via the OH⁻ route and calcined at 560 °C for 6 h: (a) 5 wt% Fe-MCM-41, (b) 10 wt% Fe-MCM-41, (c) 16 wt% Fe-MCM-41, and (d) bulk Fe₂O₃ **187**

- Figure 3.19** The XRD patterns of 5 wt% Fe-MCM-41 prepared by adding Fe(OH)₃ to the synthesis gel and carrying out the synthesis (a) at 97 °C for 45 minutes and (b) at room temperature for 4 days **189**
- Figure 3.20** XRD patterns of Co-MCM-41 prepared by the OH⁻ route at 100 °C for 48 h and calcined at 560 °C for 6 h **191**
- Figure 3.21** XRD patterns of 10 wt% Co-MCM-41 prepared hydrothermally via the hydroxide route: (a) calcined at 560 °C for 6 h, and (b) after the TPR experiment **192**
- Figure 3.22** XRD pattern of 16 wt% Co-MCM-41 (5 days at RT, OH⁻ route) **192**
- Figure 3.23** High-angle XRD patterns of Co₃O₄ (a), 16 wt% Co-MCM-41 prepared at RT for 5 days (b), and 16 wt% Co-MCM-41 prepared at 100 °C for 2 days (c) **193**
- Figure 3.24** XRD patterns of 16 wt% Me-MCM-41 prepared via the NaOH precipitate route: Me = Co (a), Fe (b) and Ru (c). All materials calcined at 560 °C for 6 h **194**
- Figure 3.25** HRTEM micrograph (a) and EDS (b) of 16 wt% Fe-MCM-41 prepared by IWI method. After overnight drying at 110 °C, the sample was calcined at 560 °C for 6 h **197**
- Figure 3.26** HRTEM micrograph of 5 wt% Fe-MCM-41 prepared by IWI on *sec*-Si-MCM-41 **198**
- Figure 3.27** HRTEM micrograph (a) and EDS (b) of 14 wt% Fe-MCM-41 material made from TEOS and urea at 80-90 °C for 24 h **199**
- Figure 3.28** HRTEM micrograph of 7.5 wt% Fe-silica material made by the aerosol route at 125 °C **200**
- Figure 3.29** HRTEM micrograph of 3 wt% Fe-MCM-41 prepared at 80 °C for 6 h. The material was then calcined at 500 °C for 12 h **200**
- Figure 3.30** HRTEM micrographs of two different regions of 5 wt% Fe-MCM-51 prepared via the OH⁻ route at 100 °C for 2 days **201**
- Figure 3.31** TPR profiles of 16 wt% Fe-MCM-41 prepared by IWI: (a) calcined at 450 °C for 12 h, (b) calcined at 560 °C for 6 h, and (c) bulk Fe₂O₃ reference **202**
- Figure 3.32** TPR profiles of (a) 5 wt% Fe-MCM-41 prepared by IWI method using *sec*-Si-MCM-41 as a support, calcined at 560 °C for 6 h, (b) bulk Fe₂O₃ **203**

Figure 3.33 TPR profiles of (a) 16 wt% Fe-MCM-41 prepared by adding $\text{Fe}^{3+}(\text{aq})$ to the synthesis gel 2 h after mixing (but prior to hydrothermal synthesis and calcination at $560\text{ }^{\circ}\text{C}$ for 6 h), and (b) bulk Fe_2O_3 **204**

Figure 3.34 TPR profiles of (a) 16 wt% Fe-MCM-41 prepared hydrothermally from $\text{Fe}^{3+}(\text{aq})$ and Si-MCM-41 as a SiO_2 source followed by calcination at $560\text{ }^{\circ}\text{C}$ for 6 h, (b) bulk Fe_2O_3 **205**

Figure 3.35 TPR profile of (a) Fe_2O_3 and (b) 8.8 wt% Fe-MCM-41 prepared by HNO_3 -mediated incorporation of Fe(III) (2 days at $100\text{ }^{\circ}\text{C}$) and calcined at $560\text{ }^{\circ}\text{C}$ for 6 h **206**

Figure 3.36 TPR profiles of Fe-MCM-41 prepared via NaOH precipitate ($100\text{ }^{\circ}\text{C}$ for 2 days): (a) 5 wt% Fe, (b) 10 wt% Fe, and (c) bulk Fe_2O_3 **207**

Figure 3.37 TPR profiles of 16 wt% Fe-MCM-41 prepared via the OH^- route at $100\text{ }^{\circ}\text{C}$ for 5 days: (a) calcined at $450\text{ }^{\circ}\text{C}$ for 12 h, and (b) calcined at $560\text{ }^{\circ}\text{C}$ for 6 h **208**

Figure 3.38 The TPR profiles of (a) 16 wt% Fe-MCM-41 prepared by delayed addition of $\text{Fe}(\text{OH})_3$ to the synthesis gel ($100\text{ }^{\circ}\text{C}$ for 2 days) and (b) bulk Fe_2O_3 **209**

Figure 3.39 TPR profiles of 16 wt% Fe-MCM-41 prepared at $100\text{ }^{\circ}\text{C}$ for 2 days via the OH^- precipitate route: (a) Na_2CO_3 and (b) $(\text{HOCH}_2\text{CH}_2)_3\text{N}$ as precipitants **210**

Figure 3.40 TPR profiles of (a) 5 wt% Fe-MCM-41 prepared via NaOH precipitation of Fe^{3+} at RT for 4 days and (b) bulk Fe_2O_3 **211**

Figure 3.41 TPR profiles of Co_3O_4 : (a) synthesized in this work, (b) reported by Wu et al **212**

Figure 3.42 TPR profiles of (a) 16 wt% Co-MCM-41 prepared by IWI with a 1 M HNO_3 solution of Fe^{3+} and calcined at $560\text{ }^{\circ}\text{C}$ for 6 h, and (b) bulk Co_3O_4 **213**

Figure 3.43 TPR profiles of Co-MCM-41 prepared via OH^- precipitates at $100\text{ }^{\circ}\text{C}$ for 2 days: (a) 5 wt% Co, (b) 10 wt% Co, and (c) bulk Co_3O_4 . All Co-MCM-41 were calcined at $560\text{ }^{\circ}\text{C}$ for 6 h **214**

Figure 3.44 TPR profiles of 10 wt% Co-MCM-41 prepared via the OH^- route at $100\text{ }^{\circ}\text{C}$ for 2 days: (a) calcined at $560\text{ }^{\circ}\text{C}$ for 6 h, (b) calcined at $450\text{ }^{\circ}\text{C}$ for 12 h and (c) bulk Co_3O_4 **215**

Figure 3.45 TPR profiles of (a) Fe_2O_3 and (b) (7.8 wt% Fe, 11.5 wt% Co)-MCM-41 prepared at $100\text{ }^{\circ}\text{C}$ for 2 days using a HNO_3 solution of the metal precursors, and calcined at $560\text{ }^{\circ}\text{C}$ for 6 h **216**

- Figure 3.46** TPR profile of (1.9 wt% Au, 6.5 wt% Fe)-MCM-41 prepared by coprecipitation of Au(III) and Fe(III) with water-glass prior to hydrothermal synthesis at 100 °C for 5 days, calcined at 560 °C for 6 h **217**
- Figure 3.47** Room temperature X-band ESR spectra of 5 wt% Fe-MCM-41 prepared at 100 °C for 2 days, as a function of calcination temperature: (a) as-synthesized, (b) 300 °C for 6 h, (c) 400 °C for 6 h, and (d) 560 °C for 6 h **218**
- Figure 3.48** ESR spectrum of as-synthesized 8.8 wt% Fe-MCM-41 prepared by room temperature synthesis for 5 days with a HNO₃ solution of Fe(III) **219**
- Figure 3.49** ESR spectrum of 8.8 wt% Fe-MCM-41 prepared at 100 °C for 2 days using Fe(III) in maleic acid solution, followed by calcination at 560 °C for 6 h **220**
- Figure 3.50** ESR spectrum of calcined (560 °C for 6 h) 8.8 wt% Fe-MCM-41 prepared at RT for 5 days with Fe(III) in oxalic acid solution **221**
- Figure 3.51** The ESR spectrum of 16 wt% Fe-MCM-41 prepared by IWI with a 1 M HNO₃ solution of Fe(III), and calcined at 560 °C for 6 h **222**
- Figure 3.52** ESR spectrum of 16 wt% Ru-MCM-41 prepared at 100 °C for 2 days using the OH⁻ synthesis route, and calcined at 560 °C for 6 h **222**
- Figure 3.53** ESR spectra of 16 wt% Co-MCM-41 prepared by IWI with HNO₃ solution of Co(II): (a) dried overnight at 110 °C, and (b) calcined at 560 °C for 6 h **224**
- Figure 3.54** ESR spectra of 16 wt% Co-MCM-41 prepared by one-pot synthesis via the OH⁻ route under different conditions: (a) 100 °C for 48 h, calcined at 560 °C for 6 h, (b) RT synthesis for 5 days, uncalcined **224**
- Figure 3.55** Raman spectra of Si-MCM-41 in the framework region: (a) primary Si-MCM-41 and (b) *sec*-Si-MCM-41 (prepared using calcined Si-MCM-41 as a SiO₂ source) **225**
- Figure 3.56** Raman spectra of Si-MCM-41 showing the OH stretching region: (a) primary Si-MCM-41 and (b) secondary Si-MCM-41 **226**
- Figure 3.57** Framework Raman spectra of 5 wt% Fe-MCM-41 (2 days at 100 °C): (a) as-synthesized, (b) calcined at 300 °C for 6 h, (c) calcined at 400 °C for 6 h, and (d) calcined at 560 °C for 6 h **227**
- Figure 3.58** Raman spectra of 5 wt% Fe-MCM-41 (2 days at 100 °C) in the OH region: (a) as-synthesized, (b) calcined at 400 °C for 6 h, and (c) calcined at 560 °C for 6 h **228**

Figure 3.59 Variation of the Raman OH band (3476 cm^{-1}) area of Fe-MCM-41 prepared at $100\text{ }^{\circ}\text{C}$ for 2 days using HNO_3 for iron incorporation. All samples were calcined at $560\text{ }^{\circ}\text{C}$ for 6 h **229**

Figure 3.60 Framework Raman spectra of 16 wt% Fe-MCM-41 prepared with Si-MCM-41 as a SiO_2 source ($100\text{ }^{\circ}\text{C}$ for 2 days) and calcined at $560\text{ }^{\circ}\text{C}$: (a) *sec*-Si-MCM-41 reference sample, (b) calcined for 3 h, and (c) calcined for 6 h **230**

Figure 3.61 Raman spectra of 16 wt% Fe-MCM-41 prepared by the TMAOH precipitate route: (a) as-synthesized, (b) calcined at $560\text{ }^{\circ}\text{C}$ for 6 h **231**

Figure 3.62 Comparative Raman spectra of 16 wt% Co-MCM-41 prepared by IWI from nitric acid solution, and hydrothermally via the $\text{Co}(\text{OH})_2$ route: (a) Framework region and (b) OH region. All samples were calcined at $560\text{ }^{\circ}\text{C}$ for 6 h **232**

Figure 3.63 IR spectra (KBr pellet) fo Fe-MCM-41 prepared at $100\text{ }^{\circ}\text{C}$ for 48 h using HNO_3 -assisted incorporation of Fe(III): (a) Si-MCM-41, (b) 1.9 wt% Fe-MCM-41, (c) 5.5 wt% Fe-MCM-41, and (d) 8.8 wt% Fe-MCM-41. All materials calcined at $560\text{ }^{\circ}\text{C}$ for 6 h **233**

CHAPTER 4

Figure 4.1 Variation of CO oxidation activity as a function of Au cluster size for the model Au/ TiO_2 (001)/Mo(100) system **248**

Figure 4.2 XRD patterns of 1.92 wt% Au/6.5 wt% Fe-MCM-41 prepared by direct hydrothermal synthesis at $100\text{ }^{\circ}\text{C}$ for 5 days, from a water-glass coprecipitate of the metal precursors **261**

Figure 4.3 XRD pattern of 3 wt% Au/5 wt% Fe/MCM-41 prepared by coprecipitating Au(III) and Fe(III) with a Na_2CO_3 solution in the presence of calcined Si-MCM-41 that was synthesized at $120\text{ }^{\circ}\text{C}$ for 3 days. The material was oven-dried at $120\text{ }^{\circ}\text{C}$ for 15 minutes prior to XRD analysis **262**

Figure 4.4 XRD patterns of 1.6 wt% Au/0.73 wt% Fe/MCM-41 (a) and 1.5 wt% Au/5 wt% Fe/MCM-41 (b) prepared by coprecipitating Au(III) and Fe(III) with Na_2CO_3 (aq) in the presence of calcined Si-MCM-41 that was synthesized at $120\text{ }^{\circ}\text{C}$ for 3 days. Both materials were air-dried before XRD measurements **263**

Figure 4.5 XRD pattern of 1.5 wt% Au/5 wt% Co/MCM-41 prepared by coprecipitating Au(III) and Co(II) with Na_2CO_3 (aq) in the presence of preformed Si-MCM-41 that was synthesized at $120\text{ }^{\circ}\text{C}$ for 3 days **264**

Figure 4.6 HRTEM micrograph (a) and PSD (b) of 1.285 wt% Au/MCM-41 prepared by direct synthesis at $96\text{ }^{\circ}\text{C}$ for 3 h. The synthesis gel was initially aged at room temperature in a PP bottle before carrying out the hydrothermal synthesis, and the final material was calcined at $500\text{ }^{\circ}\text{C}$ for 12 h **268**

Figure 4.7 HRTEM image (a) and particle size distribution (b) of 2.6 wt% Au/2.96 wt% Fe-MCM-41 prepared in situ at 80 °C for 6 h and calcined at 500 °C for 12 h **269**

Figure 4.8 HRTEM image (a) and PSD (b) of 5 wt% Au/Si-MCM-41 prepared by precipitating Au(III) with (en) in the presence of calcined Si-MCM-41, calcined at 400 °C for 4 h **270**

Figure 4.9 HRTEM image (a) and PSD (b) of 1 wt% Au/3 wt% Fe-MCM-41 prepared by precipitating Au(III) with en solution in the presence of calcined 3 wt% Fe-MCM-41, calcined at 400 °C for 4 h **272**

Figure 4.10 HRTEM image (a) and PSD (b) of 2.57 wt% Au/3 wt% Fe-MCM-41 prepared by precipitating Au(III) with en solution in the presence of calcined 3 wt% Fe-MCM-41, calcined at 400 °C for 4 h **273**

Figure 4.11 HRTEM image (a) and PSD (b) of 5 wt% Au/3 wt% Fe-MCM-41 prepared by precipitating Au(III) with en solution in the presence of calcined 3 wt% Fe-MCM-41, calcined at 400 °C for 4 h **274**

Figure 4.12 HRTEM image (a) and PSD (b) of 5wt% Au/5 wt% Fe-MCM-41 prepared by precipitating Au(III) with en solution in the presence of calcined 5 wt% Fe-MCM-41, followed by calcination at 400 °C for 4 h **275**

Figure 4.13 HRTEM image (a) and PSD (b) of 5 wt% Au/5 wt% Fe-MCM-41 prepared by precipitating Au(III) with en solution in the presence of preformed 5 wt% Fe-MCM-41, then treated to incipient wetness with a dilute base solution (0.27 % NaBH₄/0.89 % NaOH/8.85 % H₂O) prior to calcination at 400 °C for 4 h **276**

Figure 4.14 HRTEM image (a) and PSD (b) of 5 wt% Au/14 wt% Fe-MCM-41 prepared by precipitating Au(III) with en in the presence of calcined 14 wt% Fe-MCM-41, followed by calcination at 380 °C for 6 h **277**

Figure 4.15 HRTEM image (a) and PSD (b) of 1 wt% Au/5 wt% Co-MCM-41 prepared by precipitating Au(III) with en in the presence of 5 wt% Co-MCM-41, followed by calcination at 400 °C for 4 h **278**

Figure 4.16 HRTEM image (a) and PSD (b) of 5 wt% Au/5 wt% Co-MCM-41 prepared by precipitating Au(III) with en in the presence of preformed 5 wt% Co-MCM-41, calcined at 400 °C for 4 h **279**

Figure 4.17 The HRTEM image of 2.28 wt% Au/CTAB-Si-MCM-41 prepared by ethylenediamine precipitation of Au(III). The material is in its uncalcined state **280**

Figure 4.18 HRTEM image (a) and PSD (b) of 2.28 wt% Au/CTAB-Si-MCM-41 prepared by precipitating Au(III) with en in the presence of the as-synthesized Si-MCM-41, followed by calcination at 500 °C for 12 h **281**

Figure 4.19 HRTEM image (a) and PSD (b) of 2.67 wt% Au/3 wt% Fe-MCM-41 prepared by precipitating Au(III) with urea in the presence of 3 wt% Fe-MCM-41, calcined at 400 °C for 4 h **283**

Figure 4.20 HRTEM image (a) and PSD (b) of 1.1 wt% Au/3 wt% Fe-MCM-41 prepared by reducing Au(III) with sodium citrate in the presence of calcined 3 wt% Fe-MCM-41, calcined at 325 °C for 6 h **284**

CHAPTER 5

Figure 5.1 CO conversion as a function of temperature for different supported Au catalysts: Au on wormhole mesoporous silica, Au on hexagonally ordered mesoporous silica, Au on mesoporous titania calcined at 150 °C, and Au on mesoporous titania calcined at 200 °C **304**

Figure 5.2 The catalyst testing set-up for the CO oxidation reaction **307**

Figure 5.3 Light-off curve for 1.285 wt% Au/Si-MCM-41 prepared by prior aging the synthesis gel at room temperature for 20 h, followed by treatment at 96 °C for 6 h and 500 °C calcination at 500 °C for 12 h **309**

Figure 5.4 Light-off curve for 2.28 wt% Au/Si-MCM-41 prepared from AuCl₄⁻ and as-synthesized Si-MCM-41 via the (en) route. Material calcined at 500 °C for 12 h **310**

Figure 5.5 Light-off curve for 5 wt% Au/Si-MCM-41 prepared by (en) deposition-precipitation of AuCl₄⁻ onto precalcined Si-MCM-41. The catalyst system was then calcined at 400 °C for 4 h **311**

Figure 5.6 The light-off curves of Au/5 wt% Co-MCM-41 prepared by DP with (en) solution and calcination at 400 °C for 4 h: The effect of Au content **313**

Figure 5.7 The light-off curves of 1.48 wt% Au/5 wt% Co-MCM-41 prepared via the (en) deposition route and subjected to two different calcination processes. Neither HRTEM nor BET analysis was done on these samples and therefore, no average Au particle diameter has been determined **314**

Figure 5.8 The light-off curves for Au/3 wt% Fe-MCM-41 prepared by direct hydrothermal synthesis at 80 ± 2 °C for 6 h, followed by calcination at 500 °C for 12 h: The effect of Au content **315**

Figure 5.9 TOS curve for CO oxidation using 5 wt% Au/3 wt% Fe-MCM-41 prepared by hydrothermal synthesis at 80 ± 2 °C for 6 h, followed by calcination at 500 °C for 12 h. Measurements were performed at 22 °C **316**

Figure 5.10 The light-off curves for Au/3 wt% Fe-MCM-41 prepared by (en) deposition of Au(III) onto 3 wt% Fe-MCM-41, showing the effect of Au content. All samples were calcined at 400 °C for 4 h **317**

Figure 5.11 Light-off curves for 5 wt% Au-containing materials prepared by the (en) route, showing the effect of the amount of Fe in the support. All materials were calcined at 400 °C for 4 h **319**

Figure 5.12 Light-off curves for differently treated 5 wt% Au/5 wt% Fe-MCM-41 materials prepared via the (en) route: Effect of NaBH₄ treatment prior calcination at 400 °C for 4 h **321**

Figure 5.13 CO conversion versus time on stream for 5 wt% Au/5 wt% Fe-MCM-41 prepared by ethylenediamine deposition of Au(III) onto preformed 5 wt% Fe-MCM-41, treated with NaBH₄ and then calcined at 400 °C for 4 h **322**

Figure 5.14 The light-off curve for 10 wt% Au/5 wt% Fe-MCM-41 prepared by ethylenediamine deposition onto preformed 5 wt% Fe-MCM-41, calcined at 325 °C for 6 h **323**

Figure 5.15 The light-off curve for 5 wt% Au/14 wt% Fe-MCM-41 prepared via ethylenediamine deposition of Au(III) onto preformed 14 wt% Fe-MCM-41, calcined at 350 °C for 6 h **324**

Figure 5.16 Effect of metal identity on the light-off temperatures of 5 wt% Au catalysts prepared by ethylenediamine deposition of Au(III) on various supports. All materials calcined at 400 °C for 4 h **325**

Figure 5.17 The Arrhenius plots for the CO oxidation reaction using 5 wt% Au catalysts supported on Si-MCM-41, 5 wt% Fe-MCM-41 and 5 wt% Co-MCM-41. The materials were prepared via the ethylenediamine deposition route and calcined at 400 °C for 4 h **326**

Figure 5.18 Light-off curves for the Au-containing materials prepared by urea deposition-precipitation of Au(III) onto preformed 3 wt% Fe-MCM-41, calcined at 400 °C for 4 h **328**

Figure 5.19 Light-off curves for Au/5 wt% Fe-MCM-41 materials prepared by CP of Au(III) and Fe(III) with NaOH at 90 °C, calcined at 400 °C for 4 h **329**

Figure 5.20 Light-off curve for 1.07 wt% Au/3 wt% Fe-MCM-41 prepared by sodium citrate reduction at 80 °C, calcined at 325 °C for 6 h **330**

Figure 5.21 Light-off curves for uncalcined Au-containing materials prepared by coprecipitation in the presence of Si-MCM-41, showing the effect of Au loading **331**

Figure 5.22 Light-off curves for uncalcined Au-containing materials prepared by coprecipitation of Au(III) and Fe(III) in the presence of preformed Si-MCM-41, showing the effect of Fe content **332**

Figure 5.23 Light-off curves for uncalcined 1.5 wt% Au/Me-MCM-41 materials (Me = Fe or Co) prepared by coprecipitation in the presence of Si-MCM-41, showing the effect of metal identity on the activity of the catalyst **333**

LIST OF TABLES

CHAPTER 1

Table 1.1 Composition of synthesis mixtures for the formation of various M41S phases	4
Table 1.2 Iron contents and H ₂ consumption of different Fe-MCM-41 samples	38

CHAPTER 2

Table 2.1 Room temperature synthesis of Si-MCM-41: a_0 versus synthesis time	107
Table 2.2 Effect of gel SiO ₂ /CTAB mole ratio on the structure of Si-MCM-41	109
Table 2.3 XRD properties of sec-Si-MCM-41 (100 °C for 4 days)	128
Table 2.4 BET surface area (S_{BET}) versus crystallization temperature (3 days synthesis) for Si-MCM-41	136
Table 2.5 Si-MCM-41 properties: Effect of mineral acid identity	139
Table 2.6 The effect of additives to the synthesis gel on the surface area of Si-MCM-41	140
Table 2.7 Effect of gel R_{SiO_2} on S_{BET} of Si-MCM-41	140

CHAPTER 3

Table 3.1 Effects of Fe loading on the XRD properties of Fe-MCM-41 prepared by IWI	170
Table 3.2 Effect of calcination temperature on impregnated 16 wt% Fe-MCM-41	170
Table 3.3 XRD data for 16 wt% Fe-MCM-41 made with calcined Si-MCM-41 (which was made from a mixture of fumed SiO ₂ and water-glass as SiO ₂ source) as SiO ₂ source	177
Table 3.4 XRD data for 16 wt% Fe-MCM-41 made with calcined Si-MCM-41 (which was made from only water-glass as SiO ₂ precursor) as SiO ₂ source	177
Table 3.5 HNO ₃ -assisted Co(II) incorporation into the MCM-41 synthesis gel, and its effect on the properties of the resulting Co-MCM-41 materials	183

Table 3.6 Variation of the lattice parameter (a_0) of 16 wt% Fe-MCM-41 with the identity of the precipitant for Fe(III) **186**

Table 3.7 Variation of the lattice parameter and BET surface area of Fe-MCM-41 with the Fe content. The materials were calcined at 560 °C for 6 h **188**

Table 3.8 Variation of a_0 and S_{BET} with Co content for Co-MCM-41 prepared via the OH⁻ route at 100 °C for 2 days (calcined at 560 °C for 6 h) **190**

Table 3.9 XRD and BET surface area data for 16 wt% Me-MCM-41 (Me = Si, Fe, Co and Ru) prepared by the metal hydroxide route at different temperatures **195**

Table 3.10 A comparison of a_0 values of 16 wt% Fe- and Co-MCM-41 as influenced by the synthesis method **196**

Table 3.11 Assignment of IR vibrational peaks in the Fe-containing MCM-41 materials in **Figure 3.63** **234**

CHAPTER 4

Table 4.1 Representative characterization techniques for supported Au catalysts **255**

Table 4.2 Variation of S_{BET} for Au/Me-MCM-41 (Me = Si, Co and Fe) **265**

Table 4.3 Surface areas of the Au-containing samples **266**

Table 4.4 (a) One-pot synthesized Au-containing materials calcined at 500 °C for 12 h **284**

Table 4.4 (b) Post-synthetically prepared Au-containing MCM-41 prepared via en route. Calcination was done at 400 °C for 4 h, unless stated otherwise **285**

Table 4.4 (c) Other post-synthesis methods for Au-containing materials **285**

CHAPTER 5

Table 5.1 WGC Reference Gold Catalysts **301**

Table 5.2 Correlation of preparation method, Au particle size and catalytic activity for Au/Si-MCM-41 catalysts **312**

Table 5.3 Activity and other properties of Au on 5 wt% Co-MCM-41 catalysts **314**

Table 5.4 Activity and physical properties of 1-5 wt% Au/3 wt% Fe-MCM-41 **318**

Table 5.5 Activity and physical property data for 5 wt% Au on 0-5 wt% Fe-MCM-41 **320**

Table 5.6 Correlation of activity with physical properties of 5 wt% Au on different supports (Fe- and Co-modified MCM-41) **325**

Table 5.7 Activation energy (E_a) for Au/ Me-MCM-41 (Me = Si, Fe and Co) **327**

CHAPTER 6

Table 6.1 Lattice parameters and BET data for 16 wt% Me-MCM-41 (Me = Fe, Co, Ru) **352**

LIST OF ABBREVIATIONS AND ACRONYMS

AAS	Atomic Absorption Spectrometry
BET	Brunnauer-Emmett-Teller
BJH	Barrett-Joyner-Halenda
BMS	Bimodal silica
CIT-5	California Institute of Technology number 5
CO	Carbon monoxide
CMC	Critical micelle concentration
CMK	Carbon Mesostructures at KAIST
CP	Coprecipitation
COHb	Carboxyhemoglobin
CTAB	Cetyltrimethylammonium bromide
CTMAOH	Cetyltrimethylammonium hydroxide
CVD	Chemical vapour deposition
DAM-1	Dallas Amorphous Material # 1
DP	Deposition-precipitation
DRIFTS	Diffuse Reflectance Infrared Fourier Transform Spectroscopy
DRS UV-Vis	Diffuse Reflectance Spectroscopy (UV-Vis)
DTA	Differential Thermal Analysis
EDS	Energy-dispersive X-ray spectrometry
EDTA	Ethylenediamine tetraacetate
EDX	Energy-dispersive X-ray Analysis
EHC	Electrically heated catalyst
en	Ethylenediamine

EPA	Environmental Protection Agency
EPR	Electron Paramagnetic Resonance
ESR	Electron Spin Resonance
EXAFS	Extended X-ray Absorption Fine Structure
FMMS	Functionalized Monolayers on Mesoporous Supports
FMS-16	Folded Sheet Mesoporous material, 16 designates a 16 C surfactant template
(FT)IR	Fourier Transform Infrared
FTS	Fischer-Tropsch Synthesis
g	Lande factor or gyromagnetic ratio
HCs	Hydrocarbons
HDP	Homogeneous deposition-precipitation
HDS	Hydrodesulphurization
HMS	Hexagonal mesoporous silica
(HR)TEM	High resolution transmission electron microscopy
(HR)SEM	High Resolution Scanning Electron Microscopy
ICP	Inductively-coupled plasma
IEC	Ion exchange capacity
IEP	Isoelectric point
IUPAC	International Union of Pure and Applied Chemistry
IWI	Incipient wetness impregnation
KAIST	Korea Advanced Institute of Science and Technology
LAT	Ligand-assisted templating
LCT	Liquid-crystal templating
MCM	Mobil's Composition of Matter

MFI	Mobil Five
MSU-G, -X	Michigan state university-G or X
MTS	Micelle-templated silica
NO _x	Nitrogen oxides
NMR	Nuclear Magnetic Resonance
O ₂ Hb	Oxyhemoglobin
OMS	Ordered Mesoporous Silica
ORMOSILs	Organically-Modified Silicas
PE	Polyethylene
PP	Polypropylene
PGMs	Platinum Group Metals
PHCs	Porous Clay Heterostructures
PILCs	Pillared Clays
PNNL	Pacific Northwest National Laboratory
PSD	Particle size distribution
PVD	Physical Vapour Deposition
PZC	Point of Zero Charge
RS	Raman spectroscopy
SAMMS	Self-Assembled Monolayers on Mesoporous Supports
SBA	Santa Barbara
SCTA	Sample Controlled Thermal Analysis
SDA	Structure-directing agent
SFE	Supercritical Fluid Extraction
SIB	Ship-in-a-bottle

SMSIs	Strong metal-support interactions
SV	Space velocity
T ₅₀	Light-off temperature
TBHP	Tertiarybutylhydroperoxide
TCD	Thermal conductivity detector
TEA	Triethanolamine
TEOS	Tetraethyl orthosilicate
TGA	Thermogravimetric analysis
TIE	Template ion-exchange
TMCS	Trimethyl chlorosilane
TMMPS	Tris(methoxy)mercaptopropylsilane
TMOS	Tetramethyl orthosilicate
TMS-1	Transition-metal mesoporous molecular sieves
TOS	Time on stream
TPGS	α -Tocopheryl polyethylene glycol 1000 succinate
TPR	Temperature-Programmed Reduction
TUD-1	Technical University of Delft # 1
TWC	Three-way catalyst
USY	Ultrastable Y zeolite
UTD	University of Texas at Dallas
UV-Vis	Ultraviolet and Visible spectrophotometry
VAM	Vinyl acetate monomer
VPI-5	Virginia Polytechnic Institute # 5
XANES	X-ray Absorption Near-Edge Spectroscopy

XPS	X-ray Photoelectron spectroscopy
XRD	X-ray diffraction
XRF	X-ray fluorescence
WGC	World Gold Council
WGS	Water-gas shift
ZSM-5	Zeolite Saucony Mobil # 5

SCOPE AND CONTENT OF THE THESIS

Pure silica has a neutral framework in which the Si^{4+} is tetrahedrally bonded to four bridging O atoms, and consequently cannot show cation exchange properties. Metal components can be introduced into the silica to induce cation exchange capacity, redox properties and nucleation sites for the growth or development of metal nanoparticles. This thesis examines Si-MCM-41 and metal-containing variants, i.e., Fe- and Co-MCM-41 as supports for Au catalysts. Au catalysts have recently gained popularity because of their ability to catalyze a wide range of reactions at low temperature.

Chapter 1 covers the literature on inorganic porous materials, with particular reference to addressing the issue of shape selectivity in microporous materials and improving the surface area of the resulting materials. The survey includes a discussion of the first templated synthesis of a mesoporous family of zeolitic materials, designated M41S, to which belong a range of interesting materials such as MCM-41, MCM-48 and MCM-50. The survey includes the synthesis, characterization, catalytic and technical applications of the Si-MCM-41 materials.

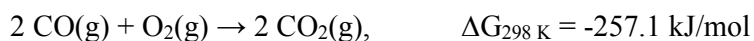
Chapter 2 presents the results of the work carried out on pure silica MCM-41 materials that were prepared in this thesis. Covered in this study are the role of various synthetic variables (i.e. optimization of the synthesis conditions) that lead to a highly ordered Si-MCM-41 with improved structural integrity, as well as enhanced thermal and hydrothermal stability. These variables include the crystallization time and reaction temperature, the synthesis gel composition (SiO_2/CTAB molar ratio and the water content), inclusion of additives as co-templates in the synthesis gel, the pH of the synthesis gel, and the nature of the silica source. These materials were characterized using X-ray diffraction (XRD) to assess structural integrity, High Resolution Transmission Electron Microscopy (HRTEM) to evaluate the microstructure of the pores, and Brunauer-Emmett-Teller (BET) surface area analysis. Conclusions at the end of the chapter are based on the findings of these characterization techniques. The optimized Si-MCM-41

materials so obtained were used as benchmarks in the synthesis of base metal-containing mesoporous MCM-41 materials described in **chapter 3**.

Chapter 3 focuses on Fe- and Co-MCM-41 materials, with particular emphasis on their synthesis and characterization. The metal precursors were introduced at various stages of the synthesis, and in various forms (i.e., as solutions or as freshly-prepared gelatinous precipitates). The synthesis was carried out under both ambient and hydrothermal temperature conditions, and the amount of the heterometal that was incorporated into the mesostructure with structural retention has been optimized. Incipient wetness impregnation was also used for the synthesis of Fe- and Co-MCM-41 derivatives. Physicochemical characterization of the resulting materials included XRD, HRTEM, BET, temperature programmed reduction (TPR), ESR spectroscopy and Raman spectroscopy. Conclusions are also included at the end of this chapter, based on the observations from these characterization techniques. These heteroatom-containing mesoporous materials, with their associated redox and cation exchange properties, were used as supports in the preparation of supported Au catalysts discussed in **chapter 4**.

Chapter 4 focuses on an investigation of different methods used to prepare supported gold nanoparticles. These methods range from deposition-precipitation, co-deposition-precipitation (both Fe(III) or Co(II) and Au(III) deposited simultaneously on Si-MCM-41), co-precipitation of Au(III) with either Fe(III) or Co(II) in the presence of a preformed Si-MCM-41, or direct one-pot hydrothermal synthesis where the metal components form part of the initial synthesis gel. Characterization of the final materials involved XRD, HRTEM, BET and EDS techniques. These materials and other related materials were evaluated for catalytic activity as described in **chapter 5**.

Chapter 5 describes the catalytic properties of the Au/Me-MCM-41 materials, with Me = Si, Fe and Co, in the reaction:



The results are interpreted in terms of the light-off temperature, i.e., the temperature at which the catalyst starts converting carbon monoxide into carbon dioxide. Conclusions based on the observed catalytic behaviour are found at the end of the chapter.

Chapter 6 presents the summary of the work done, and the main conclusions of the study entailed in this thesis.